NSRRC - J04767 (2015)

ACS APPLIED MATERIALS & INTERFACES

Research Article

www.acsami.org

Solution-Processed Zinc Oxide/Polyethylenimine Nanocomposites as Tunable Electron Transport Layers for Highly Efficient Bulk Heterojunction Polymer Solar Cells

Hsiu-Cheng Chen, Shu-Wei Lin, Jian-Ming Jiang, Yu-Wei Su, and Kung-Hwa Wei*

Department of Materials Science and Engineering, National Chiao Tung University, 300 Hsinchu, Taiwan

Supporting Information

ABSTRACT: In this study, we employed polyethylenimine-doped sol–gel-processed zinc oxide composites (ZnO:PEI) as efficient electron transport layers (ETL) for facilitating electron extraction in inverted polymer solar cells. Using ultraviolet photoelectron spectroscopy, synchrotron grazing-incidence small-angle X-ray scattering and transmission electron microscopy, we observed that ZnO:PEI composite films' energy bands could be tuned considerably by varying the content of PEI up to 7 wt %—the conduction band ranged from 4.32 to 4.0 eV—and the structural order of ZnO in the ZnO:PEI thin films would be enhanced to align perpendicular to the ITO electrode, particularly at 7 wt % PEI, facilitating electron transport vertically. We then prepared two types of bulk heterojunction systems—based on poly(3-hexylthiophene) (P3HT):phenyl-C_{61}-butryric acid methyl ester ($PC_{61}BM$) and benzo[1,2-b:4,5-b']dithiophene-thiophene-2,1,3-benzooxadiazole (PBDTTBO):phenyl-C_{71}-butryric acid methyl ester ($PC_{71}BM$)—that incorporated the ZnO:PEI composite layers. When using a composite of ZnO:PEI (93:7, w/w) as the ETL, the power conversion efficiency (PCE) of the P3HT:$PC_{61}BM$ (1:1, w/w) device improved to 4.6% from a value of 3.7% for the corresponding device that incorporated pristine ZnO as the ETL—a relative increase of 24%. For the PBDTTBO:$PC_{71}BM$ (1:2, w/w) device featuring the same amount of PEI blended in the ETL, the PCE improved to 8.7% from a value of 7.3% for the corresponding device that featured pure ZnO as its ETL—a relative increase of 20%. Accordingly, ZnO:PEI composites can be effective ETLs within organic photovoltaics.

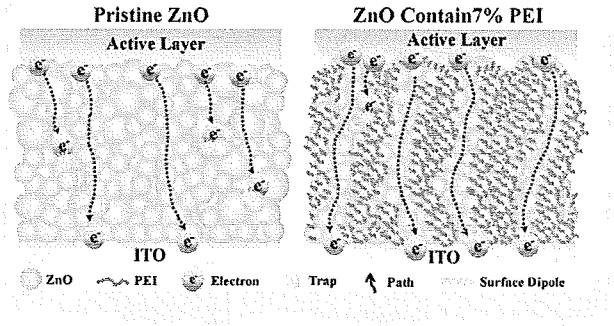

KEYWORDS: *photovoltaics, conduction band, zinc oxide: polyethylenimine nanocomposites, electron transport layer, grazing-incidence small-angle X-ray scattering*

INTRODUCTION

Organic photovoltaics (OPVs) have progressed significantly in terms of their power conversion efficiencies (PCEs) as a result of recent developments in their active layer materials, interfacial layers, and device architecture.[1−9] Although the active layer material (e.g., conjugated polymers and fullerenes) has a critical effect on the PCE, the electron transfer layer (ETL),[10−13] used as an interfacial layer between the active layer and cathode, also plays an important role because it can establish ohmic contact, modify the internal electric field, and minimize the carrier recombination rate in an OPV.[14−17] In a conventional device structure, the use of an air-sensitive ETL makes it impossible to perform the fabrication process in air, thereby necessitating that thermal evaporation techniques be performed under vacuum, increasing the complexity and fabrication cost of these devices. To solve this problem, inverted device structures have been designed, reversing the transport direction of the electrons and holes by adopting a metal having a high work function as the anode on top of the device that comprised ITO as the cathode in the bottom.[18,19]

Zinc oxide (ZnO)[20−26] has been used as an ETL in inverted OPV devices as a result of its air-stability, high transparency to visible light, high electron affinity, and tunable electrical optical properties. On the other hand, organic polymers containing simple aliphatic amine groups, namely, polyethylenimine ethoxylated (PEIE) and polyethylenimine (PEI), have also been employed as ETLs to decrease the work function of indium tin oxide (ITO) and lower the interfacial energy barrier for electron transport from the active layer to the electrode—approaching ohmic contact—by forming a thin interfacial dipole between the active layer and the ETL.[27−30] Moreover, the PCEs of devices can be improved significantly when using a conjugated polymer electrolyte as an ETL in an inverted structure.[31,32] Although ZnO is a suitable material for an ETL, the application of ZnO nanoparticles (NPs) can, however, lead to electron trapping and a high series resistance because of the presence of traps/defects with adsorbed oxygen on the NP

Received: January 20, 2015
Accepted: February 20, 2015
Published: February 20, 2015

 © 2015 American Chemical Society

DOI: 10.1021/acsami.5b00521
ACS Appl. Mater. Interfaces 2015, 7, 6273−6281

surfaces.[33,34] To overcome this obstacle, a double-layer structure that features a thin polymer layer of, for example, poly[(9,9-bis[3′-(*N*,*N*-dimethylamino)propyl]-2,7-fluorene)-*alt*-2,7-(9,9-dioctyl-fluorene)] dibromide (PFN-Br),[35,36] PEI,[37,38] or PEIE,[39−42] on top of the metal oxide layer, such as ZnO layer, can be adopted to decrease the work function of the metal oxide and further reduce the energy barrier for charge transport from the active layer to the ETL. When compared with devices based on a single metal oxide layer, the PCEs of corresponding devices containing a metal oxide/polymer bilayer as the ETL can be increased by approximately 10−40%, depending on the nature of the conjugated polymer in the active layer.

An alternative approach is to blend polymers that possess polar functional groups for interacting electrostatically with surfaces of ZnO to form composites as ETL for polymer solar cells. Nevertheless, only a few reports have appeared in which a composite ETL has been used instead of a bilayer ETL in an inverted polymer solar cell. For examples, polyvinylpyrrolidone (PVP),[28] poly(ethylene glycol) (PEG),[43] and poly(ethylene oxide) (PEO)[44] have been blended with the ZnO films to form a composite interfacial layer in a polymer solar cell; the PCEs of such devices containing a composite ETL layer can be increased by 25% relative to that of the corresponding device containing a single metal oxide layer.

In this present study, we blended a sol−gel ZnO solution with a PEI solution prior to their final consolidation into the composite layer as the ETL layer. Relative to PEIE, PEI has a higher $[N^+]/[C]$ ratio,[45] implying more protonated amino groups that can induce stronger electrostatic or dipole−dipole interactions with a ZnO surface.[37] As a result, we expected that the use of ZnO:PEI composites as ETLs would improve the device performance of inverted polymer solar cells based on two different bulk heterojunction (BHJ) active layers—poly(3-hexylthiophene) (P3HT):phenyl-C_{61}-butryric acid methyl ester ($PC_{61}BM$) (system 1) and benzo[1,2-b:4,5-*b*′]dithiophene-thiophene-2,1,3-benzooxadiazole (PBDTTBO):phenyl-C_{71}-butryric acid methyl ester ($PC_{71}BM$) (system 2). We used ultraviolet photoelectron spectroscopy (UPS) to characterize the conduction band energy of the ZnO:PEI composite layers, and grazing-incidence small-angle X-ray scattering (GISAXS) and TEM to decipher the nanostructures of our ZnO:PEI composite ETLs and to discern how the content of PEI influenced the device performance.

EXPERIMENTAL SECTION

Materials. Zinc acetate dihydrate [$Zn(CH_3COO)_2{\cdot}2H_2O$ (1 g)] and ethanolamine (0.28 g) were dissolved in 2-methoxyethanol (10 mL) under vigorous stirring for 12 h in exposure to the air.[21] This stock solution remained transparent and stable for more than one month. For preparation of the composite ETL structure device, the stock solution was mixed with a set amount of PEI (branched; average M_n = ca. 10k; Sigma−Aldrich) and stirred vigorously for 12 h. For preparation of the bilayer ETL structure device, the branched-PEI solution was diluted with DI water to give a 0.01 wt % solution. For the preparation of the BHJ systems, PBDTTBO (M_n = 268.8k; PDI = 4.4) was synthesized using a previously reported method,[46] while regioregular P3HT was purchased from Rieke Metals. $PC_{61}BM$ and $PC_{71}BM$ were obtained from FEM Technology. The blend solutions of the active layer were prepared by dissolving P3HT (10 mg mL^{-1}) with $PC_{61}BM$ (10 mg mL^{-1}) and PBDTTBO (10 mg mL^{-1}) with $PC_{71}BM$ (20 mg mL^{-1}) in dichlorobenzene (DCB), resulting in a total concentration of 4 and 3 wt %, respectively. The blend solutions were stirred continuously in a glovebox for 12 h at 90 °C to completely dissolve the polymer and fullerene.

Solar Cell Device Fabrication and Characterization. The patterned ITO glass substrate (5 Ω cm^{-2}, Merck) was cleaned through sequential ultrasonic treatments with detergent, DI water, acetone, and isopropanol and then dried under a flow of N_2. ZnO and ZnO:PEI were spin-coated on the UV ozone-treated ITO for 15 min and the annealed at 200 °C for 1 h. The ZnO/PEI structures were prepared using methods reported previously.[37] PEI layers (thickness: 2 nm) were coated on top of the ZnO layers that had been prepared through sol−gel processing. The substrates were then transferred into a dry N_2-filled glovebox. The ETLs were deposited at a thickness of approximately 40 nm, followed by deposition of the active layers. The active layers, formed from either a P3HT:$PC_{61}BM$ or PBDTTBO:$PC_{71}BM$ blend solution in DCB, were prepared in a glovebox and then spin-casted on top of the ETL film. After spin coating, the P3HT:$PC_{61}BM$ film was annealed in a glass Petri dish at room temperature for 30 min and then dried at 150 °C for 15 min under a N_2 atmosphere. The PBDTTBO:$PC_{71}BM$ film was aged for 30 min under ambient conditions prior to the deposition of the anode. The active films of P3HT:$PC_{61}BM$ and PBDTTBO:$PC_{71}BM$ had thicknesses of approximately 150 and 100 nm, respectively. The BHJ devices were fabricated with structures incorporating ITO/ZnO, ITO/ZnO:PEI (composite), or ZnO/PEI (bilayer). Device fabrication was complete after thermal evaporation of the P-type material (MoO_3, 10 nm) and the anode (Ag, 100 nm) under high vacuum (ca. 10^{-7} Torr). A shadow mask was used during the thermal evaporation process to define a device area of 0.1 cm^2.

The current density−voltage (J−V) characteristics were measured using a Keithley 2400 source meter. The photocurrent was measured under simulated AM 1.5 G illumination at 100 mW cm^{-2} using a Xe lamp-based 150-W solar simulator (Newport 66902). A calibrated Si photodiode with a KG-5 filter was employed to confirm the illumination intensity. The spectral mismatch factor was calculated by comparing the solar simulator spectrum with the AM1.5G (ASTM G173) spectrum. External quantum efficiencies (EQEs) were measured using an SRF50 system (Optosolar, Germany). A calibrated monosilicon diode was used as a reference exhibiting a response at 300−800 nm.

Electron Device Characterization of ZnO:PEI Composite Films. Space charge limited currents (SCLC) for the ZnO:PEI composite films have measured in electron only devices with a configuration of ITO/ZnO:PEI/Al (100 nm). The devices were prepared following the same procedure described in the Experimental Section for the photovoltaic devices, except that of the metal electrode. The ZnO:PEI films were prepared by spin-coating on UV ozone-treated ITO for 15 min and annealed at 200 °C for 1 h. The prepared ZnO:PEI films on ITO/glass were transferred to a vacuum evaporation chamber for the deposition of the Al (100 nm) top electrodes to complete the electron-only devices. The dark J−V characteristics measurements were performed using a Keithley 2400 source unit and calculated using SCLC Model.

Characterization of the ZnO:PEI Nanocomposite Layers. A UV−vis spectrophotometer (Hitachi U-4100) equipped with an integrating sphere was used to acquire transmission spectra. A fluorescence spectrophotometer (Hitachi F-7000) was used to record the steady state PL spectra under ambient conditions in air. The film morphology was determined through AFM in the tapping mode (Veeco Innova) under ambient conditions and the field emission scanning electron microscopy (FE-SEM, JEOL JSM-6700) under vacuum conditions. TEM images were recorded using an FEI Tecnai Spirit TWIN instrument operated at 120 keV. TEM samples were prepared on a C-covered Ni TEM micro grid. GISAXS analysis [X-ray beam energy: 8 keV (λ = 1.550 Å); incident angle: 0.2°; sample-to-detector distance: 5 m] over the sampled volume was conducted at the BL23A SWAXS end-station of the National Synchrotron Radiation Research Center (NSRRC), Hsinchu, Taiwan. The samples were prepared on 2 cm × 2 cm ITO substrates through spin-coating of ZnO:PEI solutions. The states of the Zn, O, and N atoms in the thin film were examined using XPS (ULVAC-PHI Quantera SXM). UPS was performed using He irradiation (photon energy: 21.21 eV) at a sample bias of 4 V. Synchrotron XRR analyses were performed at the

DOI: 10.1021/acsami.5b00521
ACS Appl. Mater. Interfaces 2015, 7, 6273−6281

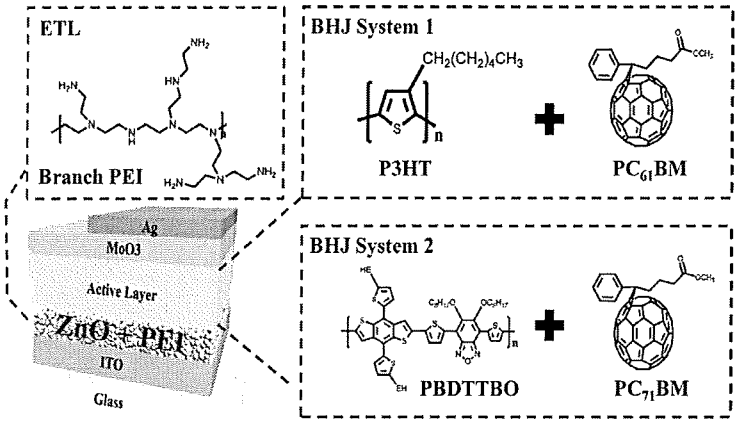

Figure 1. Chemical structures of the compounds used to prepare BHJ solar cells: branched PEI mixed in ZnO sol–gel solution as ETLs; P3HT blended with $PC_{61}BM$ and PBDTTBO blended with $PC_{71}BM$ as active layers. Lower left-hand corner: Illustration of the inverted solar cell device structure.

wiggler beamline BL-17B1 using an eight-circle diffractometer at the National Synchrotron Radiation Research Center (NSRRC), Hsinchu, Taiwan.

RESULTS AND DISCUSSION

Figure 1 displays the inverted BHJ system 1 or 2 device structure we tested in this study. As the electron donor, we used P3HT or PBDTTBO,[46] prepared through polymerization of electron-rich benzo[1,2-*b*:4,5-*b*′]dithiophene (BDT) and electron-deficient 2,1,3-benzooxadiazole (BO) moieties; as the electron acceptor, we used $PC_{61}BM$ or $PC_{71}BM$; BHJ systems 1 and 2 indicate P3HT:$PC_{61}BM$ and PBDTTBO:$PC_{71}BM$, respectively. We employed the nanocomposite ZnO:PEI layers as the underneath ETL, and deposited high-work-function molybdenum trioxide (MoO_3) on top of the bulk heterojunction (BHJ) layer as the hole transport layer. We prepared the ZnO:PEI composites through sol–gel processing of ZnO with PEI and then spin-coated them on top of the ITO. Subsequently, the active layer was spin-coated on top of the ZnO:PEI, followed by thermal evaporation of layers of molybdenum oxide (MoO_3) and silver (Ag). The detailed steps for fabricating the inverted bulk heterojunction (BHJ) polymer:fullerene solar cells with the PEI-blended ZnO layers are provided in the Experimental Section. The final device structure was glass/ITO/ZnO:PEI/BHJ system 1 or 2/MoO_3/Ag. We estimated the band gaps of our ZnO:PEI films incorporating 0%, 1%, 3%, 5%, 7%, and 9% (w/w) PEI from their transmittance spectra (see Supporting Information Figure S1), obtaining values of 3.32, 3.25, 3.29, 3.33, 3.40, and 3.39 eV, respectively. We applied UPS (photon source: He I, 21.21 eV) to determine the valence band energies of our ZnO:PEI films (see Supporting Information Figure S2). For the valence band energy, Φ, we applied the formula

$$\Phi = h\upsilon - \Delta E$$

where $h\upsilon$ was equal to 21.21 eV, with

$$\Delta E = E_1 - E_2$$

The upper emission onset energies (E_1) of the ZnO:PEI films appeared with high-energy-side shoulder tangents in the cutoff region; the lower emission onset energies (E_2) of the secondary photoelectrons appeared in the valence band region. The valence band energies for the ZnO:PEI films incorporating 0%, 1%, 3%, 5%, 7%, and 9% (w/w) PEI were determined to be 7.51, 7.53, 7.61, 7.47, 7.43, and 7.39 eV, respectively.

Figure 2 presents the energy level diagram for a device containing an ETL with a particular PEI content, an active

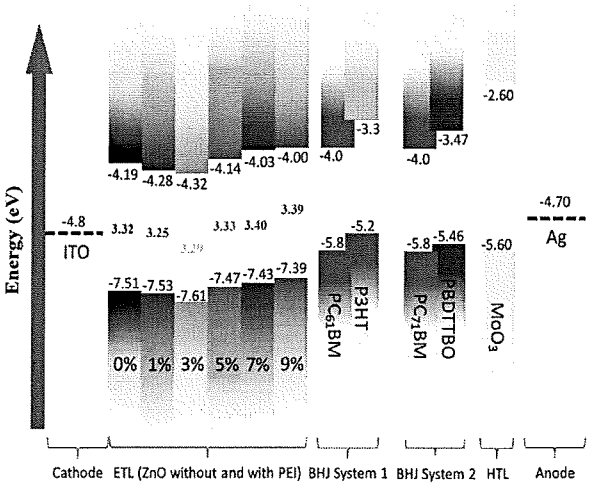

Figure 2. Energy levels of ZnO in the presence of PEI at various weight ratios, as determined from UPS and UV–vis measurements; energy levels for all other materials (P3HT, PBDTTBO, $PC_{61}BM$, $PC_{71}BM$, MoO_3) were taken from the literature.

layer, an HTL, and electrodes. The conduction band level could be calculated from the band gap and valence band level. The conduction band levels for the ZnO:PEI composite films in the range between 4.0 and 4.19 eV (see Supporting Information Table S1) were closer to the energy level of the lowest unoccupied molecular orbital (LUMO), 4.0 eV, of $PC_{61}BM$ and $PC_{71}BM$. Thus, the conduction band level of ZnO:PEI was aligned well with the LUMO energy level of the fullerene, leading to an interface that provided almost ohmic contact. Therefore, the energy level of the ZnO:PEI composite films could be adjusted to form an ideal ETL.

DOI: 10.1021/acsami.5b00521
ACS Appl. Mater. Interfaces 2015, 7, 6273–6281

To investigate the passivation effect of PEI modification on the surface defects of the ZnO films, we recorded the photoluminescence (PL) spectra of our ZnO:PEI films. Figure 3 reveals that a strong emission peak appeared near the band

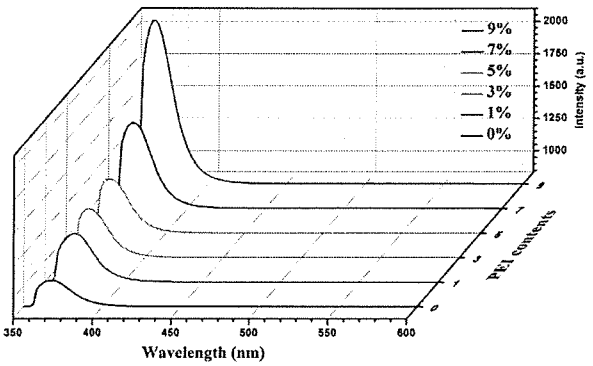

Figure 3. PL spectra of ZnO:PEI nanocomposite films incorporating PEI at various contents (0%, 1%, 3%, 5%, 7%, 9%). The conduction band edge emission appeared near 380 nm; almost no broad emission from defects appeared in the range from 450 to 600 nm.

edge at 364 nm, arising from recombination of excitons or radiative annihilation of excitons, while no apparent emission appeared near 535 nm owing to trap emission or surface recombination,[2,22,47] indicating that very few oxygen vacancy defects[48,49] were present in our ZnO thin films. The PL peak emission intensity increased upon increasing the ratio of incorporated PEI. Therefore, we suspected that the impact of oxygen vacancy defects on the overall device efficiency would be negligible. Typically, in a solar cell device, a decrease in the content of traps in the electron transport layer would presumably decrease the possibility of trap-assisted interfacial recombination of carriers and, consequently, enhance the value of short current density (J_{sc}) and the fill factor (FF), thereby improving the power conversion efficiency (PCE) of the device.[44,50] The UV–vis absorption spectra of various film structures: a ZnO:PEI/active layer film, a composite ZnO:PEI film, and a ZnO/PEI bilayer film (see Supporting Information Figure S3). Notably, the ZnO:PEI composite layer and ZnO/PEI bilayer provided similar or almost overlapping optical absorption spectra. The SEM images reveal that the pristine sample featured ripples on its surface; increasing the PEI content (1–5%) lessened the formation of ripples, whereas granular features appeared in the presence of 7% PEI (see Supporting Information Figure S4).

Figure 4 presents AFM surface topography images of the ZnO:PEI composite layers containing various amounts of PEI. We observed continuous textured and root-like structures for the pristine ZnO surface and those containing 1% and 9% PEI (Figure 4a,b,f). In contrast, the surface topographies of ZnO:PEI and ZnO/PEI featured finely dispersed particles (Figure 4e and Supporting Information Figure S5b). Notably, the presence of PEI decreased the surface roughness from 6.7 nm for pristine ZnO film to 4.6 nm for a 7% PEI in ZnO blend, potentially increasing the physical contact and inducing strong molecular dipoles between the ITO electrode and the active layer, leading to improved PCEs. In contrast, the ETL had a rougher surface, root-mean-square (RMS) roughness of 5.8 nm, when its PEI content was 9%, up from 4.6 nm for the film containing 7% PEI. A smooth film would feature fewer traps,

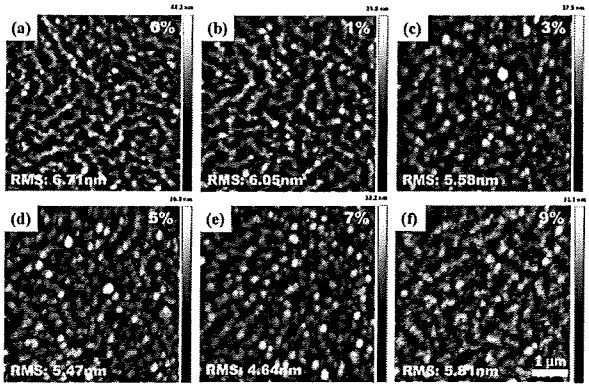

Figure 4. AFM topographic images of ZnO:PEI blends films incorporating PEI at contents of (a) 0, (b) 1, (c) 3, (d) 5, (e) 7, and (f) 9 wt %.

thereby decreasing the probability of recombination. Hence, a decrease in roughness of a ZnO film would presumably contribute to an increase in the FF. The variation in the surface morphology may have been caused by the change in the surface properties of the ZnO NPs after blending with PEI.

To understand the electronic structure of the ZnO:PEI composite films, we used X-ray photoelectron spectroscopy (XPS) to measure the surface electronic structures and depth profiles of our films. The high-resolution scans of the spectra of the Zn, O, and N atoms. The spectra of the ZnO:PEI films reveal that the Zn 2p3/2 peaks appeared at 1022 eV, the O 1s peaks near 531.4 and 533.0 eV, and the N peaks near 400 eV (see Supporting Information Figure S6). The signals suggested that the Zn atoms existed in the completely oxidized state, even though the Zn binding energy decreased slightly after blending with PEI. The O 1s peak having the lowest binding energy represents the O atoms of O^{2-} ions on the ZnO wurtzite structure of a hexagonal Zn^{2+} ion array,[51] surrounding Zn atoms with their full components; the component having the highest binding energy represents the O atoms associated with the chemisorbed oxygen ions on the ZnO surface.[52] We did not observe a very pronounced change in the nature of the bonding of the O atoms. We did, however, observe that increasing the amount of PEI led to a significant increase in the signal surface of the N atoms. Our results are consistent with those reported by Woo and Kim et al., who found that the N moieties appeared after stacking PEI on top of ZnO.[37] Comparing the series of spectra recorded upon varying the amount of added PEI, we observed a shoulder peak representing protonated amino groups after we had added 7% PEI, suggesting that the electrostatic dipoles on the surface of the ZnO:PEI (7%) sample would be stronger than those of the samples prepared at other ratios. The literature suggests that a higher [N+]/[C] ratio provides an interfacial dipole of stronger intensity, attributable to protonated amino groups (which induce electrostatic dipoles) and to C atoms (which interrupt self-assembly of protonated amino groups) in the polymer interfacial layers.[45] To determine the mixed PEI distribution, we measured XPS depth profiles. The N atoms were distributed uniformly in the ETL layer (see Supporting Information Figure S7). We also used X-ray reflectance (XRR) to examine the changes in surface roughness. The X-rays that penetrated the ZnO:PEI thin films would be reflected at the thin film–substrate interface, thereby creating an interference pattern. We

DOI: 10.1021/acsami.5b00521
ACS Appl. Mater. Interfaces 2015, 7, 6273–6281

could take advantage of the resulting period of oscillations in the XRR pattern, also known as Kiessig fringes, to determine the film thickness or roughness, in which the intensity of its reflected X-rays will drop off rapidly (lower slope) upon increasing the angle of incidence if a film surface is rough.[53] Among our tested samples, the XRR curves of the 7%PEI-blended ZnO films exhibited the most striking oscillations and lower slopes, providing direct evidence that PEI treatment decreased the roughness of the films (see Supporting Information Figure S8).

Although a clear indication of the structural changes of a film surface can be obtained using real-space imaging techniques, these structures might not extend into the inner film volume. Moreover, it is quite challenging to examine the changes in length scales of the nanostructures that form during the mixing of ZnO with PEI at various contents. Grazing-incidence small-angle X-ray scattering (GISAXS) has been used previously to analyze the nanoscale phase separation of P3HT and PCBM after annealing, as well as the effects of the sizes of the PCBM clusters and P3HT crystallites in BHJ solar cells.[54] This technique is a nondestructive, noncontact structural probe that does not require any special techniques for sample preparation; therefore, it is suitable for in situ experiments.[55] Figure 5 displays the 2D scattering patterns obtained from synchrotron GISAXS measurements of each of our samples. In these scattering patterns, the specular reflection (at an exit angle equal to the incident angle) was shielded by a beamstop to avoid oversaturation of the detector. In addition, we also installed a rod-shaped beamstop shielding the region along q_y = 0 to allow for the measurement of the q_y region.[56−58] Other than the specular peak, another high intensity peak, known as the Yoneda peak (line cut in the q_y and q_z directions: see Figure S9 in the Supporting Information), appeared at the critical angle of each material.[59] Another interesting feature observed in the signals of films containing 1% and 3% PEI was the azimuthal scattering ring (marked by the white dashed curve in Figure 5b). When more than 3% PEI was present, however, this ring was absent and, instead, prominent Bragg scattering rods appeared along the q_z direction, indicating an improvement in structural order in the direction perpendicular to the substrate. We therefore concluded that a thin film containing 7% PEI would possess an internal structure that is favorable for electron transport because the structural order of ZnO in the ZnO:PEI thin films would be aligned perpendicular to the ITO electrode. Indeed, the scattering intensity from the film incorporating 7% PEI was higher than those from the films prepared with other proportions with the same data acquisition time and beam-stops. Figure 6 displays TEM images of our ZnO:PEI films. The bright and dark regions correspond to ZnO- and PEI-rich domains, respectively, because of differences in their electron scattering densities. A fine dispersion is clearly visible in the image of the film incorporating 7% PEI (Figure 6e). Nevertheless, an increase in the aggregate domain is clearly visible upon increasing the content of PEI in the hybrid films. Accordingly, blending with PEI changed not only the surface morphology of the ZnO film but also its inner structure.

Furthermore, we determined the electron mobility (μ) across these films by applying single carrier space charge limited conduction (SCLC) model on the electron-only device that has the structure of ITO/ETL/Al. The SCLC plots reveal that the electron mobility in the vertical direction increased significantly upon increasing the PEI content—from 5.78 × 10^{-6} for the device incorporating a layer of pristine ZnO to 1.80 × 10^{-5} m^2 V^{-1} s^{-1} for the device incorporating a layer of 7 wt % PEI in ZnO—increasing the PEI content thereafter to 9% caused the electron mobility decrease to 9.07 × 10^{-6} m^2 V^{-1} s^{-1} (see Supporting Information Figure S10 and Table S1). These results correspond to the fact that structural order of ZnO in the ZnO:PEI thin films is aligned vertically to the ITO electrode quite well, which facilitates electron transport vertically.

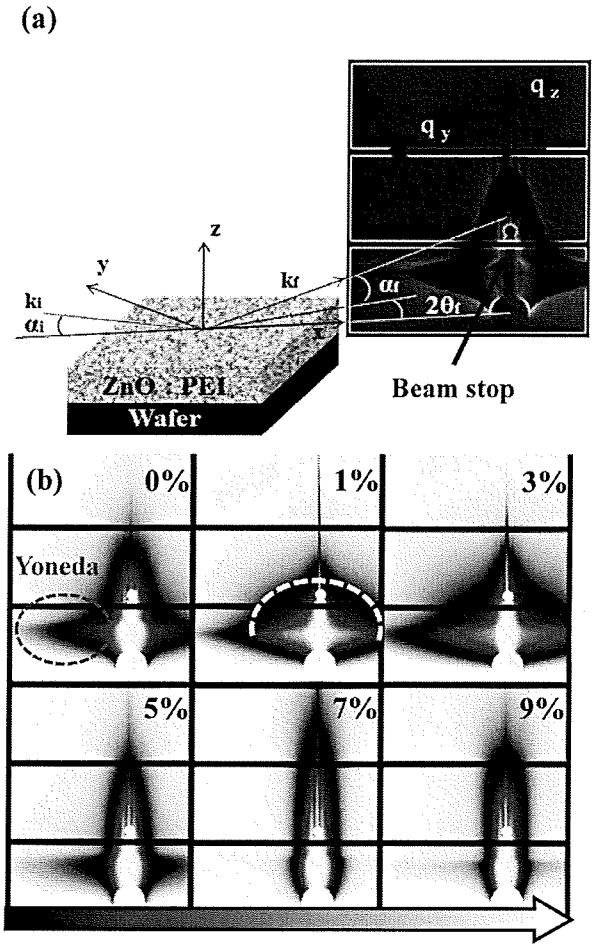

Figure 5. (a) Schematic representation of the GISAXS geometry. Incident X-rays had a wave vector ki; due to scattering, the wavevector changed to kf. The momentum transfer due to scattering is denoted as q. (b) 2D GISAXS patterns of ZnO films containing of PEI at 0%, 1%, 3%, 5%, 7%, and 9% (w/w). The specular peak for each sample was shielded by a circular beamstop. The red oval in (b) indicates the exemplary position at the Yoneda peak. The white dashed arc highlights the azimuthal scattering rings present for the samples containing 1% and 3% (w/w) PEI. Line-cut profiles along the q_y and q_z direction are presented in Figure S9.

We investigated the photovoltaic properties of inverted BHJ solar cells having the structure ITO/ETL/BHJ system 1 or 2/MoO_3/Ag. We optimized BHJ systems 1 and 2 in terms of the blend weight ratio and concentration in the active layer; furthermore, we controlled the active layer thickness by adopting the same spin speed during each device fabrication procedure. The composition of the ETL greatly affected the device performance. Figure 7 presents the illuminated (AM 1.5G irradiation, 100 mW cm^{-2}) current−voltage (J−V)

DOI: 10.1021/acsami.5b00521
ACS Appl. Mater. Interfaces 2015, 7, 6273−6281

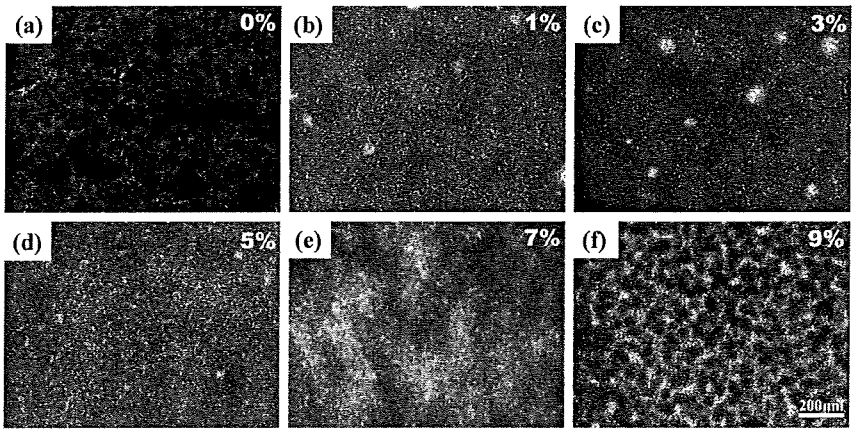

Figure 6. TEM images of ZnO:PEI nanocomposite films incorporating PEI at contents of (a) 0%, (b) 1%, (c) 3%, (d) 5%, (e) 7%, and (f) 9% (w/w).

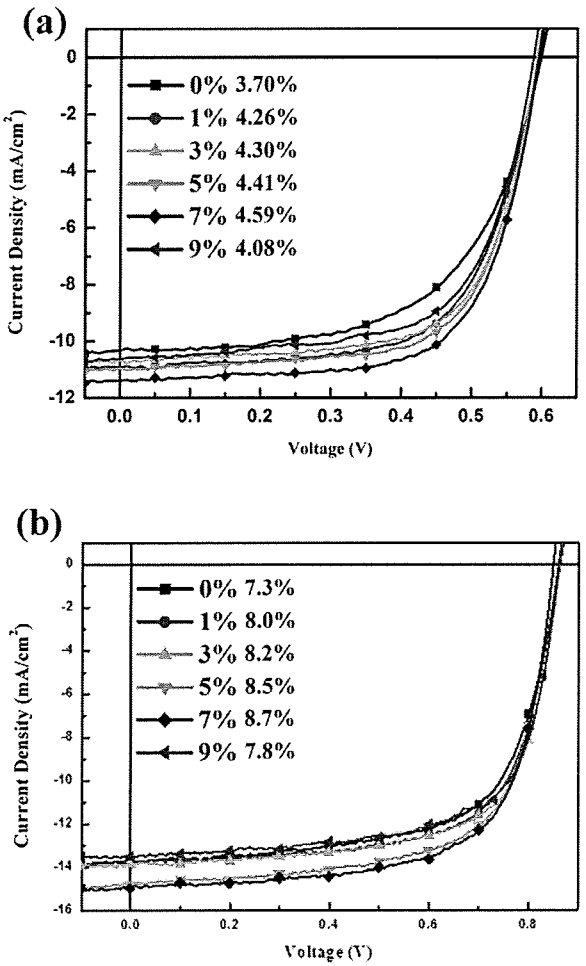

Figure 7. J–V characteristics of inverted solar cells containing (a) P3HT:$PC_{61}BM$ and (b) PBDTTBO:$PC_{71}BM$ as active layers, both with and without ETLs containing PEI at various contents.

characteristics of the P3HT:$PC_{61}BM$ and PBDTTBO:$PC_{71}BM$ solar cells incorporating various ZnO:PEI ETLs; Table 1 lists the corresponding device parameters. The reference devices,

Table 1. Device Performances of Inverted P3HT:$PC_{61}BM$ and PBDTTBO:$PC_{71}BM$ Cells

ETL	active layer	V_{oc}[a] [V]	J_{sc}[b] [mA cm^{-2}]	FF[c] [%]	η[d] [%]
ZnO:PEI (0%)	P3HT:$PC_{61}BM$	0.60	10.3	60	3.7
ZnO:PEI (1%)	P3HT:$PC_{61}BM$	0.60	10.8	65	4.2
ZnO:PEI (3%)	P3HT:$PC_{61}BM$	0.59	10.9	67	4.3
ZnO:PEI (5%)	P3HT:$PC_{61}BM$	0.59	11.1	67	4.4
ZnO:PEI (7%)	P3HT:$PC_{61}BM$	0.60	11.4	67	4.6
ZnO:PEI (9%)	P3HT:$PC_{61}BM$	0.59	10.6	65	4.1
ZnO/PEI (2 nm)	P3HT:$PC_{61}BM$	0.60	10.9	66	4.3
ZnO:PEI (0%)	PBDTTBO:$PC_{71}BM$	0.85	13.3	65	7.3
ZnO:PEI (1%)	PBDTTBO:$PC_{71}BM$	0.86	13.7	68	8.0
ZnO:PEI (3%)	PBDTTBO:$PC_{71}BM$	0.86	14.0	69	8.2
ZnO:PEI (5%)	PBDTTBO:$PC_{71}BM$	0.85	14.6	69	8.5
ZnO:PEI (7%)	PBDTTBO:$PC_{71}BM$	0.85	14.7	70	8.7
ZnO:PEI (9%)	PBDTTBO:$PC_{71}BM$	0.85	13.6	63	7.8
ZnO/PEI (2 nm)	PBDTTBO:$PC_{71}BM$	0.86	13.7	68	8.1

[a]V_{oc}: open-circuit voltage. [b]J_{sc}: short-circuit density. [c]FF: fill factor. [d]η: powder conversion efficiency.

featuring ZnO as the cathode buffer layer, for P3HT:$PC_{61}BM$ and PBDTTBO:$PC_{71}BM$ displayed open circuit voltages (V_{oc}) of 0.60 and 0.85 V, respectively; values of J_{sc} of 10.3 and 13.3 mA cm^{-2}, respectively; FFs of 60% and 65%, respectively; and PCEs of 3.7% and 7.3%, respectively. The device performance improved considerably after adding PEI into ZnO to form the ETL as a result of enhanced short-current density and fill factor. The optimal P3HT:$PC_{61}BM$ device was prepared with ETLs comprising 7% PEI blended with ZnO; it displayed value of V_{oc} of 0.59 V; value of J_{sc} of 11.4 cm^{-2}; FF of 67%; and PCEs of 4.59% from a value of 3.7% for the corresponding device incorporating pristine ZnO as the ETL—a relative increase of

DOI: 10.1021/acsami.5b00521
ACS Appl. Mater. Interfaces 2015, 7, 6273–6281

24%. The optimal PBDTTBO:$PC_{71}BM$ device was also prepared with ETLs comprising 7% PEI blended with ZnO; it displayed a value of V_{oc} of 0.85 V; value of J_{sc} of 14.7 cm^{-2}; FF of 70%; and PCEs of 8.7% from a value of 7.3% for the corresponding device incorporating pristine ZnO as the ETL—a relative increase of 20%. Increasing the PEI loading beyond 7% decreased the device performance; for example, when the PEI content was 9%, the P3HT:$PC_{61}BM$ and PBDTTBO:$PC_{71}BM$ devices displayed lower values of J_{sc} (10.6 and 13.6 mA cm^{-2}, respectively) and lower FFs (65% and 63%, respectively), resulting in PCEs of 4.08% and 7.8%, respectively. The EQE curves provided integrated values of J_{sc} that were close to those measured directly from the $J-V$ curves of the optimized BHJ systems 1 and 2 (see Supporting Information Figure S11). We also fabricated another set (five devices in each case) of control devices having the structures glass/ITO/ZnO (2 nm)/PEI/BHJ system 1 or 2/MoO_3/Ag, and chose the best performing ones for comparison (see Supporting Information Figure S12). Surprisingly, the illuminated $J-V$ characteristics of the devices incorporated ZnO:PEI systems were better than those of the devices incorporated the bilayer (ZnO/PEI) ETL systems, with values of J_{sc} and V_{oc} greater than those of corresponding devices containing either ZnO or ZnO/PEI as the ETL. This might be explained by the fact that there is only one interface between the active layer and the ZnO:PEI composite layer, whereas there are two interfaces between the active layer and the ZnO/PEI bilayer, reducing the efficiency of carrier transport vertically slightly because of interfacial traps.

CONCLUSIONS

Through systematic characterizations of these ZnO:PEI nanocomposite ETL films using ultraviolet photoelectron spectroscopy, synchrotron grazing-incidence small-angle X-ray scattering and reflectivity, atomic force microscopy, and transmission electron microscopy, we found that the ZnO:PEI nanocomposites' physical, optical, electronic, morphological, and inner structural properties are superior to that of the pristine ZnO film as electron transport layers for inverted polymer solar cells. In particular, we found that N atoms (electron-donating) from the PEI component existed not only on the surface after the blending process, but they were also distributed in the ETL layer; hence the blending of PEI within the ZnO films improved the surface roughness of the ZnO layer and enhanced the structural order of ZnO in the ZnO:PEI layer perpendicular to the ITO electrode, thereby increasing the electron mobility in the vertical direction significantly. As a result, introducing PEI-blended ZnO as the ETL between the active layer P3HT:$PC_{61}BM$ and PBDTTBO:$PC_{71}BM$ and the ITO substrate improved the interfacial smoothness, band alignment (near ohmic contact), and electron mobility, thereby enhancing the photovoltaic performance of the devices. For instance, the values of J_{sc} and FF of inverted BHJ system solar cells featuring a composite of ZnO:PEI (93:7, w/w) as the ETL were improved considerably compared to those of the device incorporating the pristine ZnO layer; the power conversion efficiency (PCE) of the P3HT:$PC_{61}BM$ (1:1, w/w) device using a composite of ZnO:PEI (93:7, w/w) improved to 4.6% from a value of 3.7% for the corresponding device incorporating pristine ZnO as the ETL—a relative increase of 24%. For the PBDTTBO:$PC_{71}BM$ (1:2, w/w) device featuring the same composite of ZnO:PEI (93:7, w/w) as the ETL, the PCE improved to 8.7% from a value of 7.3% for the corresponding device featuring pure ZnO as its ETL—a relative increase of 20%. Therefore, ZnO:PEI composites can be effective ETLs within organic photovoltaics.

ASSOCIATED CONTENT

Supporting Information

Table showing energy level diagram, surface roughness, and electron mobility for ZnO:PEI nanocomposite films. Determination of the energy gap and valence band of ZnO:PEI by transmittance spectra and UPS analysis. Optical absorption spectra and EQE data of P3HT:$PC_{61}BM$ and PBDTTBO:$PC_{71}BM$ systems incorporating PEI (7%) as ETLs. SEM image and XRR shown the ZnO incorporating different PEI ratios. Determination of the Zn, O, N atoms of electron structures and depth profiles by XPS results. Electron mobility determined by electron-only device and calculated by SCLC model. Performance of P3HT:$PC_{61}BM$ and PBDTTBO:$PC_{71}BM$ devices based on pristine ZnO, ZnO:PEI, and ZnO/PEI. This material is available free of charge via the Internet at http://pubs.acs.org.

AUTHOR INFORMATION

Corresponding Author

*E-mail: khwei@mail.nctu.edu.tw.

Notes

The authors declare no competing financial interest.

ACKNOWLEDGMENTS

We thank the National Science Council, Taiwan, for financial support (NSC 102-3113-P-009-002), and Ming-Wei Lin and Yu-Ling Lai from Dr. Yao-Jane Hsu's group (NSRRC) for help with the UPS measurements.

REFERENCES

(1) Steim, R.; Kogler, F. R.; Brabec, C. J. Interface Materials for Organic Solar Cells. *J. Mater. Chem.* **2010**, *20*, 2499–2512.

(2) Lai, T.-H.; Tsang, S.-W.; Manders, J. R.; Chen, S.; So, F. Properties of Interlayer for Organic Photovoltaics. *Mater. Today* **2013**, *16*, 424–432.

(3) Su, Y.-W.; Lan, S.-C.; Wei, K.-H. Organic Photovoltaics. *Mater. Today* **2012**, *15*, 554–562.

(4) Liu, S.; Zhang, K.; Lu, J.; Zhang, J.; Yip, H.-L.; Huang, F.; Cao, Y. High-Efficiency Polymer Solar Cells via the Incorporation of an Amino-Functionalized Conjugated Metallopolymer as a Cathode Interlayer. *J. Am. Chem. Soc.* **2013**, *135*, 15326–15329.

(5) Liao, S.-H.; Jhuo, H.-J.; Cheng, Y.-S.; Chen, S.-A. Fullerene Derivative-Doped Zinc Oxide Nanofilm as the Cathode of Inverted Polymer Solar Cells with Low-Bandgap Polymer (PTB7-Th) for High Performance. *Adv. Mater.* **2013**, *25*, 4766–4771.

(6) Zhou, L.; Ou, Q.-D.; Chen, J.-D.; Shen, S.; Tang, J.-X.; Li, Y.-Q.; Lee, S.-T. Light Manipulation for Organic Optoelectronics Using Bio-inspired Moth's Eye Nanostructures. *Sci. Rep.* **2014**, *4*, 4040.

(7) Li, C.-Z.; Chang, C.-Y.; Zang, Y.; Ju, H.-X.; Chueh, C.-C.; Liang, P.-W.; Cho, N.; Ginger, D. S.; Jen, A. K. Y. Suppressed Charge Recombination in Inverted Organic Photovoltaics via Enhanced Charge Extraction by Using a Conductive Fullerene Electron Transport Layer. *Adv. Mater.* **2014**, *26*, 6262–6267.

(8) Chen, J.-D.; Cui, C.; Li, Y.-Q.; Zhou, L.; Ou, Q.-D.; Li, C.; Li, Y.; Tang, J.-X. Single-Junction Polymer Solar Cells Exceeding 10% Power Conversion Efficiency. *Adv. Mater.* **2015**, *27*, 1035–1041.

(9) Liao, S.-H.; Jhuo, H.-J.; Yeh, P.-N.; Cheng, Y.-S.; Li, Y.-L.; Lee, Y.-H.; Sharma, S.; Chen, S.-A. Single Junction Inverted Polymer Solar Cell Reaching Power Conversion Efficiency 10.31% by Employing Dual-Doped Zinc Oxide Nano-Film as Cathode Interlayer. *Sci. Rep.* **2014**, *4*, 6813.

DOI: 10.1021/acsami.5b00521
ACS Appl. Mater. Interfaces 2015, 7, 6273–6281

(10) Liu, C.-M.; Su, M.-S.; Jiang, J.-M.; Su, Y.-W.; Su, C.-J.; Chen, C.-Y.; Tsao, C.-S.; Wei, K.-H. Distribution of Crystalline Polymer and Fullerene Clusters in Both Horizontal and Vertical Directions of High-Efficiency Bulk Heterojunction Solar Cells. *ACS Appl. Mater. Interfaces* **2013**, *5*, 5413−5422.

(11) Su, M.-S.; Kuo, C.-Y.; Yuan, M.-C.; Jeng, U. S.; Su, C.-J.; Wei, K.-H. Improving Device Efficiency of Polymer/Fullerene Bulk Heterojunction Solar Cells Through Enhanced Crystallinity and Reduced Grain Boundaries Induced by Solvent Additives. *Adv. Mater.* **2011**, *23*, 3315−3319.

(12) Chiu, M.-Y.; Jeng, U. S.; Su, M.-S.; Wei, K.-H. Morphologies of Self-Organizing Regioregular Conjugated Polymer/Fullerene Aggregates in Thin Film Solar Cells. *Macromolecules* **2010**, *43*, 428−432.

(13) Lai, Y.-Y.; Cheng, Y.-J.; Hsu, C.-S. Applications of Functional Fullerene Materials in Polymer Solar Cells. *Energy Environ. Sci.* **2014**, *7*, 1866−1883.

(14) Yip, H.-L.; Jen, A. K. Y. Recent Advances in Solution-Processed Interfacial Materials for Efficient and Stable Polymer Solar Cells. *Energy Environ. Sci.* **2012**, *5*, 5994−6011.

(15) Chen, L.-M.; Xu, Z.; Hong, Z.; Yang, Y. Interface Investigation and Engineering - Achieving High Performance Polymer Photovoltaic Devices. *J. Mater.Chem.* **2010**, *20*, 2575−2598.

(16) Ma, H.; Yip, H.-L.; Huang, F.; Jen, A. K. Y. Interface Engineering for Organic Electronics. *Adv. Funct. Mater.* **2010**, *20*, 1371−1388.

(17) Intemann, J. J.; Yao, K.; Li, Y.-X.; Yip, H.-L.; Xu, Y.-X.; Liang, P.-W.; Chueh, C.-C.; Ding, F.-Z.; Yang, X.; Li, X.; Chen, Y.; Jen, A. K. Y. Highly Efficient Inverted Organic Solar Cells Through Material and Interfacial Engineering of Indacenodithieno[3,2-b]thiophene-Based Polymers and Devices. *Adv. Funct. Mater.* **2014**, *24*, 1465−1473.

(18) Lloyd, M. T.; Olson, D. C.; Lu, P.; Fang, E.; Moore, D. L.; White, M. S.; Reese, M. O.; Ginley, D. S.; Hsu, J. W. P. Impact of Contact Evolution on the Shelf Life of Organic Solar Cells. *J. Mater. Chem.* **2009**, *19*, 7638−7642.

(19) He, Z.; Zhong, C.; Su, S.; Xu, M.; Wu, H.; Cao, Y. Enhanced Power-Conversion Efficiency in Polymer Solar Cells Using an Inverted Device Structure. *Nat. Photonics* **2012**, *6*, 591−595.

(20) Park, H.-Y.; Lim, D.; Kim, K.-D.; Jang, S.-Y. Performance Optimization of Low-Temperature-Annealed Solution-Processable ZnO Buffer Layers for Inverted Polymer Solar Cells. *J. Mater. Chem. A* **2013**, *1*, 6327−6334.

(21) Sun, Y.; Seo, J. H.; Takacs, C. J.; Seifter, J.; Heeger, A. J. Inverted Polymer Solar Cells Integrated with a Low-Temperature-Annealed Sol-Gel-Derived ZnO Film as an Electron Transport Layer. *Adv. Mater.* **2011**, *23*, 1679−1683.

(22) Chen, S.; Small, C. E.; Amb, C. M.; Subbiah, J.; Lai, T.-h.; Tsang, S.-W.; Manders, J. R.; Reynolds, J. R.; So, F. Inverted Polymer Solar Cells with Reduced Interface Recombination. *Adv. Energy Mater.* **2012**, *2*, 1333−1337.

(23) Kim, K.-D.; Lim, D. C.; Hu, J.; Kwon, J.-D.; Jeong, M.-G.; Seo, H. O.; Lee, J. Y.; Jang, K.-Y.; Lim, J.-H.; Lee, K. H.; Jeong, Y.; Kim, Y. D.; Cho, S. Surface Modification of a ZnO Electron-Collecting Layer Using Atomic Layer Deposition to Fabricate High-Performing Inverted Organic Photovoltaics. *ACS Appl. Mater. Interfaces* **2013**, *5*, 8718−8723.

(24) Bai, S.; Jin, Y.; Liang, X.; Ye, Z.; Wu, Z.; Sun, B.; Ma, Z.; Tang, Z.; Wang, J.; Würfel, U.; Gao, F.; Zhang, F. Ethanedithiol Treatment of Solution-Processed ZnO Thin Films: Controlling the Intragap States of Electron Transporting Interlayers for Efficient and Stable Inverted Organic Photovoltaics. *Adv. Energy Mater.* **2014**, 1401606.

(25) Sanchez, S.; Berson, S.; Guillerez, S.; Lévy-Clément, C.; Ivanova, V. Toward High-Stability Inverted Polymer Solar Cells with an Electrodeposited ZnO Electron Transporting Layer. *Adv. Energy Mater.* **2012**, *2*, 541−545.

(26) Liang, Z.; Zhang, Q.; Wiranwetchayan, O.; Xi, J.; Yang, Z.; Park, K.; Li, C.; Cao, G. Effects of the Morphology of a ZnO Buffer Layer on the Photovoltaic Performance of Inverted Polymer Solar Cells. *Adv. Funct. Mater.* **2012**, *22*, 2194−2201.

(27) Kang, H.; Lee, J.; Jung, S.; Yu, K.; Kwon, S.; Hong, S.; Kee, S.; Lee, S.; Kim, D.; Lee, K. Self-Assembly of Interfacial and Photoactive Layers via One-Step Solution Processing for Efficient Inverted Organic Solar Cells. *Nanoscale* **2013**, *5*, 11587−11591.

(28) Zhou, Y.; Fuentes-Hernandez, C.; Shim, J.; Meyer, J.; Giordano, A. J.; Li, H.; Winget, P.; Papadopoulos, T.; Cheun, H.; Kim, J.; Fenoll, M.; Dindar, A.; Haske, W.; Najafabadi, E.; Khan, T. M.; Sojoudi, H.; Barlow, S.; Graham, S.; Brédas, J.-L.; Marder, S. R.; Kahn, A.; Kippelen, B. A Universal Method to Produce Low−Work Function Electrodes for Organic Electronics. *Science* **2012**, *336*, 327−332.

(29) Kang, H.; Hong, S.; Lee, J.; Lee, K. Electrostatically Self-Assembled Nonconjugated Polyelectrolytes as an Ideal Interfacial Layer for Inverted Polymer Solar Cells. *Adv. Mater.* **2012**, *24*, 3005−3009.

(30) Li, P.; Wang, G.; Cai, L.; Ding, B.; Zhou, D.; Hu, Y.; Zhang, Y.; Xiang, J.; Wan, K.; Chen, L.; Alameh, K.; Song, Q. High-Efficiency Inverted Polymer Solar Cells Controlled by the Thickness of Polyethylenimine Ethoxylated (PEIE) Interfacial Layers. *Phys. Chem. Chem. Phys.* **2014**, *16*, 23792−23799.

(31) Liu, J.; Wu, J.; Shao, S.; Deng, Y.; Meng, B.; Xie, Z.; Geng, Y.; Wang, L.; Zhang, F. Printable Highly Conductive Conjugated Polymer Sensitized ZnO NCs as Cathode Interfacial Layer for Efficient Polymer Solar Cells. *ACS Appl. Mater. Interfaces* **2014**, *6*, 8237−8245.

(32) Xie, C.; Chen, L.; Chen, Y. Electrostatic Self-Assembled Metal Oxide/Conjugated Polyelectrolytes as Electron-Transporting Layers for Inverted Solar Cells with High Efficiency. *J. Phys. Chem. C* **2013**, *117*, 24804−24814.

(33) Small, C. E.; Chen, S.; Subbiah, J.; Amb, C. M.; Tsang, S.-W.; Lai, T.-H.; Reynolds, J. R.; So, F. High-Efficiency Inverted Dithienogermole-Thienopyrrolodione-Based Polymer Solar Cells. *Nat. Photonics* **2012**, *6*, 115−120.

(34) Manor, A.; Katz, E. A.; Tromholt, T.; Krebs, F. C. Enhancing Functionality of ZnO Hole Blocking Layer in Organic Photovoltaics. *Sol. Energy Mater.Sol. Cells* **2012**, *98*, 491−493.

(35) Chang, Y.-M.; Leu, C.-Y. Conjugated Polyelectrolyte and Zinc Oxide Stacked Structure as an Interlayer in Highly Efficient and Stable Organic Photovoltaic Cells. *J. Mater. Chem. A* **2013**, *1*, 6446−6451.

(36) Yang, T.; Wang, M.; Duan, C.; Hu, X.; Huang, L.; Peng, J.; Huang, F.; Gong, X. Inverted Polymer Solar Cells with 8.4% Efficiency by Conjugated Polyelectrolyte. *Energy Environ. Sci.* **2012**, *5*, 8208−8214.

(37) Woo, S.; Hyun Kim, W.; Kim, H.; Yi, Y.; Lyu, H.-K.; Kim, Y. 8.9% Single-Stack Inverted Polymer Solar Cells with Electron-Rich Polymer Nanolayer-Modified Inorganic Electron-Collecting Buffer Layers. *Adv. Energy Mater.* **2014**, *4*, 1301692.

(38) Yang, D.; Fu, P.; Zhang, F.; Wang, N.; Zhang, J.; Li, C. High Efficiency Inverted Polymer Solar Cells with Room-Temperature Titanium Oxide/Polyethylenimine Films as Electron Transport Layers. *J. Mater. Chem. A* **2014**, *2*, 17281−17285.

(39) Yao, K.; Intemann, J. J.; Yip, H.-L.; Liang, P.-W.; Chang, C.-Y.; Zang, Y.; Li, Z. a.; Chen, Y.; Jen, A. K. Y. Efficient all Polymer Solar Cells from Layer-Evolved Processing of a Bilayer Inverted Structure. *J. Mater. Chem. C* **2014**, *2*, 416−420.

(40) Cha, H.-C.; Huang, Y.-C.; Hsu, F.-H.; Chuang, C.-M.; Lu, D.-H.; Chou, C.-W.; Chen, C.-Y.; Tsao, C.-S. Performance Improvement of Large-Area Roll-to-Roll Slot-Die-Coated Inverted Polymer Solar Cell by Tailoring Electron Transport Layer. *Sol. Energy Mater. Sol. Cells* **2014**, *130*, 191−198.

(41) Kyaw, A. K. K.; Wang, D. H.; Gupta, V.; Zhang, J.; Chand, S.; Bazan, G. C.; Heeger, A. J. Efficient Solution-Processed Small-Molecule Solar Cells with Inverted Structure. *Adv. Mater.* **2013**, *25*, 2397−2402.

(42) Lee, T. H.; Choi, H.; Walker, B.; Kim, T.; Kim, H.-B.; Kim, J. Y. Replacing the Metal Oxide Layer with a Polymer Surface Modifier for High-Performance Inverted Polymer Solar Cells. *RSC Adv.* **2014**, *4*, 4791−4795.

(43) Jo, S. B.; Lee, J. H.; Sim, M.; Kim, M.; Park, J. H.; Choi, Y. S.; Kim, Y.; Ihn, S.-G.; Cho, K. High Performance Organic Photovoltaic

DOI: 10.1021/acsami.5b00521
ACS Appl. Mater. Interfaces 2015, 7, 6273−6281

Cells Using Polymer-Hybridized ZnO Nanocrystals as a Cathode Interlayer. *Adv. Energy Mater.* **2011**, *1*, 690−698.
(44) Shao, S.; Zheng, K.; Pullerits, T.; Zhang, F. Enhanced Performance of Inverted Polymer Solar Cells by Using Poly(ethylene oxide)-Modified ZnO as an Electron Transport Layer. *ACS Appl. Mater. Interfaces* **2012**, *5*, 380−385.
(45) Kim, Y.-H.; Han, T.-H.; Cho, H.; Min, S.-Y.; Lee, C.-L.; Lee, T.-W. Polyethylene Imine as an Ideal Interlayer for Highly Efficient Inverted Polymer Light-Emitting Diodes. *Adv. Funct. Mater.* **2014**, *24*, 3808−3814.
(46) Jiang, J.-M.; Lin, H.-K.; Lin, Y.-C.; Chen, H.-C.; Lan, S.-C.; Chang, C.-K.; Wei, K.-H. Side Chain Structure Affects the Photovoltaic Performance of Two-Dimensional Conjugated Polymers. *Macromolecules* **2013**, *47*, 70−78.
(47) Dkhil, S. B.; Duché, D.; Gaceur, M.; Thakur, A. K.; Aboura, F. B.; Escoubas, L.; Simon, J.-J.; Guerrero, A.; Bisquert, J.; Garcia-Belmonte, G.; Bao, Q.; Fahlman, M.; Videlot-Ackermann, C.; Margeat, O.; Ackermann, J. Interplay of Optical, Morphological, and Electronic Effects of ZnO Optical Spacers in Highly Efficient Polymer Solar Cells. *Adv. Energy Mater.* **2014**, *4*, 1400805.
(48) Ye, J. D.; Gu, S. L.; Qin, F.; Zhu, S. M.; Liu, S. M.; Zhou, X.; Liu, W.; Hu, L. Q.; Zhang, R.; Shi, Y.; Zheng, Y. D. Correlation Between Green Luminescence and Morphology Evolution of ZnO Films. *Appl. Phys. A: Mater. Sci. Process.* **2005**, *81*, 759−762.
(49) Djurišić, A. B.; Choy, W. C. H.; Roy, V. A. L.; Leung, Y. H.; Kwong, C. Y.; Cheah, K. W.; Gundu Rao, T. K.; Chan, W. K.; Fei Lui, H.; Surya, C. Photoluminescence and Electron Paramagnetic Resonance of ZnO Tetrapod Structures. *Adv. Funct. Mater.* **2004**, *14*, 856−864.
(50) Yao, I. C.; Pang, L.; Tseng, T.-Y. Field Emission Properties and Reliability of ZnO Nanorod, Nanopagoda, and Nanotip Current Emitters. *IEEE Trans. Nanotechnol.* **2012**, *11*, 746−750.
(51) Ramgir, N. S.; Mulla, I. S.; Pillai, V. K. Micropencils and Microhexagonal Cones of ZnO. *J. Phys. Chem. B* **2006**, *110*, 3995−4001.
(52) De la Rosa, E.; Sepúlveda-Guzman, S.; Reeja-Jayan, B.; Torres, A.; Salas, P.; Elizondo, N.; Yacaman, M. J. Controlling the Growth and Luminescence Properties of Well-Faceted ZnO Nanorods. *J. Phys. Chem. C* **2007**, *111*, 8489−8495.
(53) Croce, P.; Devant, G.; Sere, M. G.; Verhaeghe, M. F. Thin Film Surface Studies by X-ray Reflection. *Surf. Sci.* **1970**, *22*, 173−186.
(54) Chiu, M.-Y.; Jeng, U. S.; Su, C.-H.; Liang, K. S.; Wei, K.-H. Simultaneous Use of Small- and Wide-Angle X-ray Techniques to Analyze Nanometerscale Phase Separation in Polymer Heterojunction Solar Cells. *Adv. Mater.* **2008**, *20*, 2573−2578.
(55) Müller-Buschbaum, P. The Active Layer Morphology of Organic Solar Cells Probed with Grazing Incidence Scattering Techniques. *Adv. Mater.* **2014**, *26*, 7692−7709.
(56) Kaune, G.; Memesa, M.; Meier, R.; Ruderer, M. A.; Diethert, A.; Roth, S. V.; D'Acunzi, M.; Gutmann, J. S.; Müller-Buschbaum, P. Hierarchically Structured Titania Films Prepared by Polymer/Colloidal Templating. *ACS Appl. Mater. Interfaces* **2009**, *1*, 2862−2869.
(57) Sarkar, K.; Schaffer, C. J.; Gonzalez, D. M.; Naumann, A.; Perlich, J.; Muller-Buschbaum, P. Tuning the Pore Size of ZnO Nano-Grids via Time-Dependent Solvent Annealing. *J. Mater. Chem. A* **2014**, *2*, 6945−6951.
(58) Chen, C.-M.; Liu, C.-M.; Tsai, M.-C.; Chen, H.-C.; Wei, K.-H. A Nanostructured Micellar Diblock Copolymer Layer Affects the Memory Characteristics and Packing of Pentacene Molecules in Non-Volatile Organic Field-Effect Transistor Memory Devices. *J. Mater. Chem. C* **2013**, *1*, 2328−2337.
(59) Yoneda, Y. Anomalous Surface Reflection of X Rays. *Phys. Rev.* **1963**, *131*, 2010−2013.

DOI: 10.1021/acsami.5b00521
ACS Appl. Mater. Interfaces 2015, 7, 6273−6281